Electron-optical phonon interaction and in-plane mobility in lead chalcogenide quantum-well structures

Victor Bondarenko*
Department of Theoretical Physics, Institute of Physics, National Academy of Sciences of Ukraine, 46, prospekt Nauky, Kiev-28, 252650, Ukraine

(Received 26 June 1998; revised manuscript received 11 January 1999)

The in-plane electron mobility limited by scattering from optical phonons in lead chalcogenide (PbSnTe-type) quantum-well structures is studied theoretically. It is found that the mobility decreases drastically for quantum-well widths smaller than about 200 Å. The scattering from the interface phonons is responsible for that. The nonparabolicity considerably reduces the mobility. Influence of the nonparabolicity on the mobility essentially depends upon the growth axis of the quantum-well structure. It is found that the nonparabolicity in quantum-well systems can be successfully represented by two following effects: (1) dependence of the in-plane electron effective mass upon the in-plane electron wave vector (subband nonparabolicity), and (2) dependence of the in-plane electron effective mass upon the subband number and quantum-well width (in-plane mass quantization). It is shown that, if the quantum-well width exceeds 250 Å, influence of the nonparabolicity on the mobility is actually represented by the subband nonparabolicity alone, otherwise the in-plane mass quantization effect arises. The mobility of a many-subband system is found to be limited mainly by the intrasubband scattering. The mobility of electrons in a higher subband is smaller than that in the first one, which is due to the larger in-plane effective mass and stronger scattering rates in the higher subband. The mobility is essentially affected by electrons in a higher subband, while the gap between this subband and the ground one does not exceed k_BT. The electrophonon resonance effect is also considered. [S0163-1829(99)07223-9]

I. INTRODUCTION

Electron-optical phonon interaction in polar semiconductor quantum-well (QW) structures has attracted considerable interest because of its importance for electronic properties. There have been a number of theoretical works on the electron transport in QW's taking into account the interaction between electrons and long-wavelength optical phonons and treating the effect of spatial confinement on both the electron and phonon states.[1–6]

According to the dielectric continuum model applied to layered structures (DCML),[7] phonon modes interacting with electrons in layered structures are classified as either confined LO modes or interface modes (IF) [or surface (SO) modes for a free-standing slab]. It is shown that electron scattering from the phonons does not depend much upon the geometry and dimensionality (three, two, or one) of semiconductor systems for reasonable QW widths (100 Å).[8] Particular interest has been recently to the LO-mode confinement, which can significantly affect the scattering rates, provided the scattering from the LO modes is dominant[9–15] (phonon engineering[9,16–18]).

The band mixing in QW's is taken into account through a nonparabolicity and energy-dependent boundary conditions for derivatives of the electron wave function at the potential discontinuities. Small effect of the band mixing on the wave functions is normally neglected in the first approximation. The in-plane motion and the motion in the QW growth direction appear to be coupled due to the nonparabolicity.[19–29]

There has been a single paper[6] (to our knowledge) where complexity of the phonon modes and nonparabolicity in QW's were taken into consideration to compute numerically the intrinsic electron mobility in $Ga_{0.47}In_{0.53}As$ wells. However, Ref. 6 is mostly focused on the mobility limited by different scattering mechanisms together when only the ground subband is occupied by electrons.

In this respect, IV-VI narrow-gap semiconductor QW structures are attractive for investigation because of a strong electron-phonon interaction (EPI), nonparabolicity, carrier mass anisotropy, and different valley configurations [the EPI is the dominant mobility-limiting mechanism within temperature range from 77 to 300 K and the nonparabolicity seriously affects the electron transport in bulk $Pb_{1-x}Sn_xTe$ (Ref. 30)]. Transport phenomena in such QW structures, which are interesting for both physics and device applications,[31] have not yet been investigated systematically. There is essential discrepancy between the experimental data on in-plane mobility of lead chalcogenide QW systems available in the literature,[32–35] and different quality of the samples is supposed to be responsible for that. Nevertheless, this mobility is comparable with the bulk mobility if the QW width exceeds 500 Å. The interfaces in $PbTe/Pb_{1-x}Sn_xTe$ structures are not perfect due to interdiffusion of the adjacent layers, which gives rise to a considerable roughness scattering. In this investigation we nevertheless assume the interfaces to be perfect.

In this paper, we present theoretical investigation of the scattering rate and in-plane mobility of a nondegenerate electron gas, taking the EPI to be the scattering mechanism. Two structures are studied: (1) a single rectangular $Pb_{1-x}Sn_xTe$ QW imbedded between two PbTe barriers; (2) a rectangular infinitely deep $Pb_{1-x}Sn_xTe$ QW of a $Pb_{1-x}Sn_xTe$ free-standing slab (FSS). The rectangular profile of the QW is in fact not modified by the field of nondegenerate electron gas

due to the large dielectric constant. The QW structures with axes $\langle 111\rangle$ and $\langle 001\rangle$ are studied. The electrons are assumed to occupy one and two lowest subbands. Influence of the electron energetic structure and the phonon-mode spectrum on the mobility of these low-dimensional systems is analyzed. The frequencies of the bulk LO-phonon modes for PbTe and $Pb_{1-x}Sn_xTe$ are very close to each other. That is why it seems to be correct that the phonons in $PbTe/Pb_xSn_{1-x}Te/PbTe$ QW system are assumed to be the bulk ones. A more rigorous treatment presented in this work reveals whether or not this assumption is justified and under what conditions.

The paper is organized as follows. In Sec. II A, expressions for the electron wave function and dispersion of the electron energy are discussed. Analytical expressions describing the EPI and electron conductivity are presented in the following sections: formulas for the Hamiltonian, in Sec. II B; scattering rates, in Sec. II C; conductivity tensor of a single valley and mobility of many-valley systems, in Sec. II D. The variational method is utilized for a description of the inelastic EPI because the relaxation-time approximation is not valid. The results obtained in our work are discussed: properties of electron-IF-phonon interaction, Sec. III A; effect of temperature and QW width on the EPI and electron mobility, Sec. III B; influence of the nonparabolicity on the mobility for many-subband systems with different valley configurations, Sec. III C; and the electrophonon resonance effect for a two-subband system, Sec. III D. The most important results are summarized in Sec. IV.

II. THEORY

A. Electrons

We investigate a two-subband system of a nondegenerate two-dimensional (2D) electron gas in two QW structures: (1) a $PbTe/Pb_xSn_{1-x}Te/PbTe$ structure where the intermediate $Pb_{1-x}Sn_xTe$ layer is a single rectangular QW (for $0<z<a$, z being the QW growth axis) imbedded between two semi-infinite PbTe barriers with height V_b; (2) an infinitely deep QW of $Pb_{1-x}Sn_xTe$ FSS of thickness a.

In bulk IV-VI semiconductors like PbTe there are four equivalent energetic valleys at the L points with their axes oriented along $\langle 111\rangle$ and equivalent directions. In this paper we consider two configurations with certain symmetric crystal orientations of the QW in $PbTe/Pb_xSn_{1-x}Te/PbTe$ and $Pb_{1-x}Sn_xTe$ FSS. For configuration 1, the z axis is directed along $\langle 111\rangle$ (the three ''oblique'' valleys are equivalent). For configuration 2, the z axis is directed along $\langle 100\rangle$ (all the four ''oblique'' valleys are equivalent). On account of uncertainty of the potential barrier height values,[36] configuration 1 is considered in two extreme cases. Configuration 1a: electrons are assumed to fill the $\langle 111\rangle$ valley only, while the first subbands of the ''oblique'' valleys remain empty for being too distant (Fig. 1). Configuration 1b: all the four valleys are assumed to be occupied, the minimum of the first subband of the $\langle 111\rangle$ valley is supposed to be equal to the minima of the first subbands of the three ''oblique'' valleys.

The electrons are considered separately in one valley because the intervalley coupling between various $\langle 111\rangle$ valleys in $PbTe/Pb{-}xSn_{1-x}Te$ vanishes in our approximation[37] (see also Sec. III B). Here we neglect the band-mixing effect

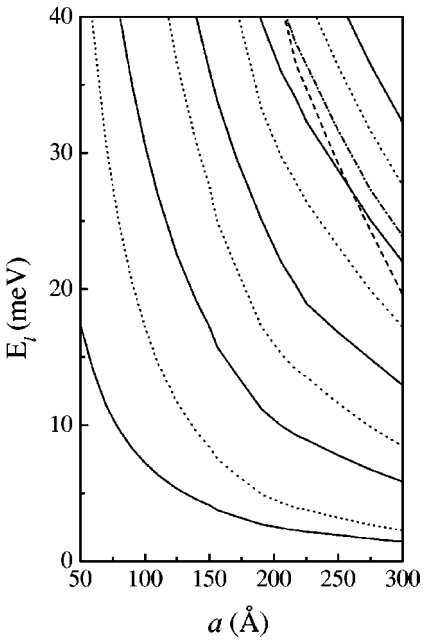

FIG. 1. Energy minima of subbands as functions of the QW width of $PbTe/Pb_{0.8}Sn_{0.2}Te/PbTe$ at $T=300$ K [according to Eq. (2)]. For the $\langle 111\rangle$ valley: solid lines—$V_b=60$ meV, dots—$V_b=\infty$. For ''oblique'' valleys: dot-dashes — configuration 1b, dashes— configuration 2. Zero energy corresponds to the bottom of the conduction band in the QW.

on the electron wave functions and restrict the consideration to a nonparabolicity in the two-band Kane's model. The eigenfunction of the effective mass Hamiltonian $\hat{H}$ describing the electron in the lth subband can be written as $|\mathbf{k}_l\rangle = \exp(i\mathbf{k}_l\mathbf{r})\mathbf{\Psi}_l(\mathbf{k}_l,z)$. Here $\mathbf{\Psi}_l(\mathbf{k}_l,z)$ is the solution of the Schrödinger equation $\hat{H}\mathbf{\Psi}_l(\mathbf{k}_l,z)=\epsilon_l\mathbf{\Psi}_l(\mathbf{k}_l,z)$, $\mathbf{k}_l$ and $\mathbf{r}$ are the 2D wave vector and the position vector of an electron in the x-y plane, and ϵ_l is the total electron energy. The Hamiltonian $\hat{H}$ is given in Ref. 20. The higher band contribution and strain influence will be omitted in this Hamiltonian. The in-plane motion is practically independent of the motion in the z direction when the nonparabolicity is not very strong, particularly for the lowest subband as our numerical calculation shows. Then $\epsilon_l=E_l+\epsilon_{\|,l}$, where E_l is the minimum energy, and $\epsilon_{\|,l}$ is the electron kinetic energy of the in-plane motion for the lth subband. The multidimensional vector of the envelope function $\mathbf{\Psi}_l(\mathbf{k}_l,z)$ can be replaced, in the first approximation, by the (normalized) conduction component $\Phi_l(z)=\Phi_{l,\mathbf{k}_l=0}(z)$, which is the eigenfunction of the one-dimensional Schrödinger equation $[\hat{H}(\mathbf{k}_l=0,\ k_z=i\partial/\partial z)+V]\mathbf{\Phi}_l=E_l\mathbf{\Phi}_l$, with V being the QW potential profile. The boundary conditions for the wave-function derivatives at the interfaces are taken energy dependent. To simplify our calculations, the $Pb_xSn_{1-x}Te$ QW is assumed to be an infinitely deep one for configurations 1b and 2, with $\Phi_l(z)=\sqrt{2/a}\sin(l\pi z/a)$ if $0<z<a$, and $\Phi_l(z)=0$ otherwise.[38]

Generally, dispersion relation ϵ_l vs $\mathbf{k}_l$ for a valley depends upon the angle θ between the axis of the valley and the QW growth direction. The general dispersion relation, describing the in-plane and z motions of electrons in the QW and in the barriers of $PbTe/Pb_xSn_{1-x}Te/PbTe$, for an ''oblique'' valley has the form

$$\tilde{\epsilon}_l = -\frac{\epsilon_g}{2} + \frac{1}{2}[\epsilon_g^2 + 4(p_z^2 K_l^2 + p_x^2 k_{x,l}^2 + p_y^2 k_{y,l}^2 + 2p_{yz}^2 K_l k_{y,l})]^{1/2}, \quad (1)$$

where $\tilde{\epsilon}_l = \epsilon_l$ for the QW, and $\tilde{\epsilon}_l = V_b - \epsilon_l$ for the barriers; ϵ_g is the bulk band-gap energy, K_l is the wave vector describing the motion in the z direction, which is independent of $\mathbf{k}_l$, and $k_l^2 = k_{x,l}^2 + k_{y,l}^2$. $p_x^2 = p_\perp^2$, $p_y^2 = p_\perp^2 \cos^2\theta + p_\parallel^2 \sin^2\theta$, $p_z^2 = p_\parallel^2 \cos^2\theta + p_\perp^2 \sin^2\theta$, and $p_{yz}^2 = (p_\perp^2 - p_\parallel^2)\sin\theta\cos\theta$, with $p_{\parallel,\perp}^2 = \hbar^2 \epsilon_g / 2m_{\parallel,\perp}^0$, where $m_{\parallel,\perp}^0 = m_0 \epsilon_g / u_{\parallel,\perp}$. Here, $u_\parallel$ and $u_\perp$ are the band-structure parameters, and m_0 is the free-electron mass. $\epsilon_l = 0$ at the bottom of the conduction band in the QW. ϵ_g, $u_\parallel$, $u_\perp$, and K_l in Eq. (1) are different for the QW and barrier. The following expressions describe the electrons in the QW.

Within the above approach the confinement energy of the lth subband is determined by Eq. (1) with $k_l = 0$

$$E_l = -\frac{\epsilon_g}{2} + \frac{1}{2}\left[\epsilon_g^2 + 4\hbar^2 K_l^2 u_\parallel \times \left(\cos^2\theta + \frac{u_\perp}{u_\parallel}\sin^2\theta\right) \Big/ 2m_0\right]^{1/2} \quad (2)$$

(note that index $\parallel$ in $\epsilon_{\parallel,l}$ implies ''parallel to the interface or to the x-y plane'' but not to $\langle 111\rangle$ as for the band parameter $u_\parallel$.)

According to Eqs. (1) and (2) we have

$$\epsilon_{\parallel,l} = \frac{1}{2}\{-\epsilon_{g,l}^* + [(\epsilon_{g,l}^*)^2 + 4(p_x^2 k_{x,l}^2 + p_y^2 k_{y,l}^2 + 2p_{yz}^2 k_{y,l} K_l)]^{1/2}\}, \quad (3)$$

where $\epsilon_{g,l}^* = \epsilon_g + 2E_l$ is the effective energy gap for the electrons in the lth subband. Expressions (1)–(3) describe the $\langle 111\rangle$ valley and the ''oblique'' valleys for configuration 1, when $\theta = 0$ and $\theta = 70.52°$ ($\cos\theta = 1/3$), respectively. They also describe all valleys for configuration 2, when $\theta = 54.76°$ ($\cos\theta = 1/\sqrt{3}$).

Equation (3) takes a simple form for the $\langle 111\rangle$ valley, when all the directions in the x-y plane are equivalent, and $p_x = p_y$, $p_{yz} = 0$

$$\frac{\hbar^2 k_l^2}{2m_{\perp,l}^*(a)} = \epsilon_{\parallel,l}\left(1 + \frac{\epsilon_{\parallel,l}}{\epsilon_{g,l}^*}\right), \quad (4)$$

with

$$m_{\perp,l}^*(a) = m_\perp^0 \frac{\epsilon_{g,l}^*}{\epsilon_g}. \quad (5)$$

The form of Eq. (4) is the same as for the usual bulk nonparabolic dispersion law where ϵ_g is replaced by $\epsilon_{g,l}^*$, and the bulk band-edge mass $m_\perp^0 = m_0 \epsilon_g / u_\perp$ is replaced by the subband edge mass $m_{\perp,l}^* = m_0 \epsilon_{g,l}^* / u_\perp$.

Equation (4) shows that within the scope of the considered approach the nonparabolicity in the QW's can be represented by two following dependencies: (a) dependence of the in-plane electron effective mass upon the in-plane electron wave vector (subband nonparabolicity), Eq. (4) where $m_{\perp,l}^*$ is assumed to be independent of a and l; (b) dependence of the in-plane electron effective mass upon QW width and subband number (size quantization of the in-plane effective mass), Eq. (5).

From Eq. (4) one can obtain the expression for the in-plane velocity effective mass

$$m_{v,l}(\epsilon_{\parallel,l}, a) = m_{\perp,l}^*(a)\left(1 + \frac{2\epsilon_{\parallel,l}}{\epsilon_{g,l}^*}\right). \quad (6)$$

Note that the size quantization affects the in-plane effective mass even in the case of parabolic subband when $m_{v,l}(\epsilon_{\parallel,l}, a) = m_{\perp,l}^*(a)$, although in the parabolic approach (from the very beginning) we cannot get Eqs. (5) and (6). Advantage of Eqs. (4), (5), and (6) is that they can be utilized for a comparison with numerical results and experimental data.

To facilitate the following calculations, it is convenient to change the integration variables from $d\mathbf{k}_l = d\mathbf{k}_{x,l} d\mathbf{k}_{y,l}$ to $d\epsilon_{\parallel,l}$. To find $k_l = k_l(\epsilon_{\parallel,l})$ we employ the coordinates $k_{x,l}^* = k_{x,l} p_x / p^*$ and $k_{y,l}^* = (k_{y,l} + \gamma / p_y) p_y / p^*$ instead of $k_{x,l}$ and $k_{y,l}$, where $\gamma = K_l p_y p_{yz}^2 / p_z^2$, and p^* is an arbitrary number with the dimension of p_x. In the new coordinates $(k_{x,l}^*)^2 + (k_{y,l}^*)^2 = (k_l^*)^2$. Then we have

$$k_l^* = \frac{1}{p^*}[\epsilon_{\parallel,l}^2 + \epsilon_{\parallel,l}\epsilon_{g,l}^* + \gamma^2]^{1/2}, \quad (7)$$

and

$$d\mathbf{k}_l = \frac{1}{2p_x p_y}[2\epsilon_{\parallel,l} + \epsilon_{g,l}^*] d\epsilon_{\parallel,l} d\vartheta, \quad (8)$$

where ϑ is the angle between $\mathbf{k}_l^*$ and $\mathbf{k}_{x,l}^*$.

Equations (7) and (8) yield a correlation between the in-plane effective masses for the $\langle 111\rangle$ valley and ''oblique'' valleys (indicated $\langle 111\rangle$ and $\langle o\rangle$, respectively)

$$m_{x,l}^{\langle o\rangle} = m_{x,l}^{\langle 111\rangle}, m_{y,l}^{\langle o\rangle} = \frac{m_{y,l}^{\langle 111\rangle}}{\cos^2\theta + (m_\perp^0 / m_\parallel^0)\sin^2\theta}, \quad (9)$$

where $m_{x,l}^{\langle 111\rangle} = m_{y,l}^{\langle 111\rangle} = m_{\perp,l}^*$.

B. Hamiltonian of the electron-phonon interaction

Using the standard techniques, we find the Hamiltonian describing a single electron in a valley at the position $\mathbf{R} = (\mathbf{r}, z)$ interacting with a phonon polarization field, i.e.,

$$\hat{H}_{e-ph}(\mathbf{R}) = \sum_\alpha \sum_{\mathbf{q}} \Gamma_\alpha(q,z)\exp(-i\mathbf{q}\mathbf{r})[\hat{a}_\alpha(\mathbf{q}) + \hat{a}_\alpha^+(-\mathbf{q})], \quad (10)$$

where

$$\Gamma_\alpha = -C_0^{1/2} G_\alpha V_\alpha. \quad (11)$$

Here $C_0 = (4\pi e^2 \hbar \omega_{l,1} a / S)(\epsilon_{\infty,1}^{-1} - \epsilon_{0,1}^{-1})$, $\mathbf{q}$ is the in-plane phonon wave vector, and S is the area of the sample in the x-y plane; $\omega_{l,\nu}$ ($\omega_{t,\nu}$) is the frequency of the bulk longitudinal (transverse) vibrations, $\epsilon_{\infty,\nu}$ is the high-frequency dielectric constant, and $\epsilon_{0,\nu}$ is the dielectric permittivity of the νth

medium. α is an index labeling the IF, SO, and LO modes. The confined LO modes are distinguished by an integer m. $\hat{a}_\alpha^+$ and $\hat{a}_\alpha$ are the operators of creation and annihilation for the αth mode.

Expressions for G_α and V_α have the following form. For the confined LO modes

$$G_{\rm lo}=[(qa)^2+(m\pi)^2]^{-1/2} \tag{12}$$

and $V_{\rm lo}=\sin(m\pi z/a)$.

For the symmetric IF modes (s_+ and s_-) and antisymmetric ones (a_+ and a_-) of the PbTe/Pb$_x$Sn$_{1-x}$Te/PbTe three-layered structure

$$G_\alpha=2^{-1/2}\left(\frac{\omega_{l,1}}{\omega_\alpha}\right)^{1/2}\frac{\omega_\alpha^2-\omega_{t,1}^2}{\omega_{l,1}^2-\omega_{t,1}^2}[qa\sinh(qa)]^{-1/2}B_\alpha^{-1} \tag{13}$$

and $V_{s\pm}=\cosh[q(z-a/2)]$, $V_{a\pm}=\sinh[q(z-a/2)]$.

For the symmetric SO modes (s) and antisymmetric ones (a) of the FSS

$$G_\alpha=\frac{1}{2}\left[\frac{\omega_{l,1}}{\omega_\alpha}\right]^{1/2}\left(1+(\epsilon_{\infty,1}-1)\frac{\omega_{l,1}^2-\omega_\alpha^2}{\omega_{l,1}^2-\omega_{t,1}^2}\right)\exp(-qa/2)\times[\tanh(qa/2)/qa]^{1/2}, \tag{14}$$

while $V_s=V_{s\pm}$ and $V_a=V_{a\pm}$. Here,

$$B_\alpha^2=1+\frac{\epsilon_{\infty,1}(\epsilon_{\infty,1}+2)}{\epsilon_{\infty,2}(\epsilon_{\infty,2}+2)}\left(\frac{\omega_{l,1}^2-\omega_\alpha^2}{\omega_{l,2}^2-\omega_\alpha^2}\right)^2\frac{\omega_{l,2}^2-\omega_{t,2}^2}{\omega_{l,1}^2-\omega_{t,1}^2}g_\alpha(qa), \tag{15}$$

where $g_\alpha(qa)$ is equal to $\tanh(qa/2)$ for the symmetric modes, and $\coth(qa/2)$ for the antisymmetric modes.

We are now able to calculate the matrix element for the electron transition between initial state $|i\rangle=|\mathbf{k}_l\rangle$ and final state $\langle f|=\langle\mathbf{k}_{l'}'|$ due to the scattering from the αth mode

$$\langle\mathbf{k}_{l'}'|\hat{H}_\alpha|\mathbf{k}_l\rangle=-\sum_{\mathbf{q}}C_0^{1/2}Q_{ll'}^\alpha\triangle(-\mathbf{k}_{l'}'+\mathbf{k}_l\pm\mathbf{q}), \tag{16}$$

where ''+'' (''−'') in the double sign ''±'' corresponds to the electron scattering with absorption (emission) of one phonon of the αth mode. The upper prime in $\langle\mathbf{k}_{l'}'|$ labels the state after the scattering while the lower prime indicates that the electron is in the l'th subband after the scattering, where $l'=l$ for the intrasubband scattering, and $l'\neq l$ for the intersubband one. Here $Q_{ll'}^\alpha=2G_\alpha J_{ll'}^\alpha(N_{0,\alpha}+\frac{1}{2}-\pm\frac{1}{2})^{1/2}$,

$$J_{ll'}^\alpha=\frac{1}{a}\int_{-\infty}^{\infty}dz\Phi_l(z)\Phi_{l'}(z)V_\alpha, \tag{17}$$

and $N_{0,\alpha}=[\exp(\hbar\omega_\alpha/k_BT)-1]^{-1}$ is the density of equilibrium phonons of the αth mode. $\triangle(x)$ is one if $x=0$ and zero otherwise.

C. Scattering rates

The scattering rate between the initial $|i\rangle$ and final $\langle f|$ electron states in a valley in the QW, due to the scattering from the αth mode, can be obtained from Fermi golden rule

$$W_\alpha(i,f)=\frac{4\pi^2}{S}\sum_{\mathbf{q}}W_\alpha^0(i,f)\triangle(-\mathbf{k}_{l'}'+\mathbf{k}_l\pm\mathbf{q})\times\delta(-\epsilon_{l'}'+\epsilon_l\pm\hbar\omega_\alpha), \tag{18}$$

where

$$W_\alpha^0(i,f)=2C_0(Q_{ll'}^\alpha)^2. \tag{19}$$

Here, ϵ_l and $\epsilon_{l'}'$ are the total electron energies before and after the event. The total scattering rate is $W(i,f)=\Sigma_\alpha W_\alpha(i,f)$.

The expression for $q^2=(\mathbf{k}_{l'}'-\mathbf{k}_l)^2$ for an arbitrary valley has the form

$$q^2=\left(\frac{p^*}{p_\perp}\right)^2\left[(k_{l'}^{*'}\cos\vartheta'-k_l^*\cos\vartheta)^2+\frac{(k_{l'}^{*'}\sin\vartheta'-k_l^*\sin\vartheta)^2}{\cos^2\theta+(u_\parallel/u_\perp)\sin^2\theta}\right]. \tag{20}$$

To calculate $W_\alpha(i,f)$ we replace the summation over $\mathbf{q}$ by integration over the polar coordinates q, φ, i.e., $(4\pi^2/S)\Sigma_{\mathbf{q}}\rightarrow\int d\mathbf{q}$ with $d\mathbf{q}=qdqd\varphi$, where φ is the angle of scattering formed between vectors $\mathbf{k}_l$ and $\mathbf{q}$. For the sake of simplicity we restrict our consideration to configuration 1a with a single $\langle 111\rangle$ valley. The standard calculation yields

$$W_\alpha(i,f)=\int d\varphi\sum_n\int dqqW_\alpha^0(i,f)|F(i,f;q,\varphi)|\,\delta(q-q_n), \tag{21}$$

where

$$F(i,f;q,\varphi)=\frac{2p_\perp^2(q\pm k_l\cos\varphi)}{(\epsilon_{g,l'}^{*2}+4p_\perp^2k_{l'}'^2)^{1/2}}. \tag{22}$$

q_n takes two values, q_+ and q_-, or briefly $q_\star$ with ''$\star$'' being either ''+'' or ''−.'' This can be written as a function of $\epsilon_{\parallel,l}$ in the form

$$q_\star=-\pm p_\perp^{-2}[(\epsilon_{\parallel,l}^2+\epsilon_{\parallel,l}\epsilon_{g,l}^*)^{1/2}\cos\varphi]\star p_\perp^{-2}\times\{(\epsilon_{\parallel,l}^2+\epsilon_{\parallel,l}\epsilon_{g,l}^*)\cos^2\varphi+\hbar\omega_\alpha[\hbar\omega_\alpha\pm(2\epsilon_{\parallel,l}+\epsilon_{g,l}^*)]-(\epsilon_{g,l'}^{*2}-\epsilon_{g,l}^{*2})/4\}^{1/2}. \tag{23}$$

q_- is not considered for the absorption since it is negative.

The expressions under the square root in Eq. (23) are demanded to be positive that gives the condition for the scattering angle φ: $-\varphi_0\leqslant\varphi\leqslant\varphi_0$. φ_0 is different for emission and absorption, i.e.,

$$\varphi_0=\arccos\{[(\epsilon_{g,l'}^{*2}-\epsilon_{g,l}^{*2})/4-\hbar\omega_\alpha\times(\hbar\omega_\alpha\pm(2\epsilon_{\parallel,l}+\epsilon_{g,l}^*))]/[\epsilon_{\parallel,l}^2+\epsilon_{\parallel,l}\epsilon_{g,l}^*]\}^{1/2}, \tag{24}$$

and the initial kinetic energy of the electron has to exceed some minimum value, $\epsilon_{\parallel,l}\geqslant E_{l'}-E_l\pm\hbar\omega_\alpha$.

For the parabolic dispersion law ($\epsilon_{g,l}^*\gg\epsilon_{\parallel,l}$), the expression for φ_0 for the scattering with emission is of the form $\varphi_0=\arccos\sqrt{[\hbar\omega_\alpha-(E_l-E_{l'})]/\epsilon_{\parallel,l}}$. The nonparabolicity re-

duces this scattering angle interval. Note that, if $\epsilon^*_{g,l'} \leqslant \epsilon^*_{g,l}$, the scattering event with absorption is isotropic and can occur with any initial kinetic energy of the electron.

Expressions for the scattering rates to the angle interval $(\varphi + d\varphi)$ for emission (em) and absorption (ab) are of the form

$$W^{(em)}_{\alpha}(i,f)d\varphi = 2 \sum_{q_n^{(em)} = q_{\pm}^{(em)}} q_n^{(em)} W^0_{\alpha}(i,f) \times |F(i,f;q,\varphi)|_{q=q_n^{(em)}} d\varphi, \quad (25)$$

$$W^{(ab)}_{\alpha}(i,f)d\varphi = 2q_+^{(ab)} W^0_{\alpha}(i,f)|F(i,f;q,\varphi)|_{q=q_+^{(ab)}} d\varphi. \quad (26)$$

In the above equations, the symmetry of the scattering to $(\varphi + d\varphi)$ and $-(\varphi + d\varphi)$ angle intervals is taking into account by the factor 2 .

D. Conductivity tensor for one valley, mobility for many-valley systems

To obtain the conductivity tensor we utilize the variational method[39] for 2D systems, because the relaxation time approximation is not valid for an inelastic EPI. According to this method the distribution function describing the electrons in the lth subband of a valley is taken as a sum of symmetric and antisymmetric parts, i.e.,

$$f(\mathbf{p}_l) = f_0(\epsilon_{\parallel,l})[1 + \phi(\mathbf{p}_l)]. \quad (27)$$

Here $f_{0,l}(\epsilon_{\parallel,l}) = A_{0,l} \exp(-\epsilon_{\parallel,l}/k_B T)$ is the Maxwell distribution function, $\mathbf{p}_l = \hbar \mathbf{k}_l$, and

$$\phi(\mathbf{p}_l) = \sum_{j,\beta} C^{\beta}_{j,l} p_{l,\beta} \epsilon^j_{\parallel,l}, \quad (28)$$

with $|\phi(\mathbf{p}_l)| \ll 1$. $C^{\beta}_{j,l}$ is a factor, j is an integer, and β is the Cartesian coordinate, x or y. It is sufficient to restrict the power series in Eq. (28) to $j = 0$ and 1 (see the closing reference in Ref. 39).

The collision term, describing all possible transitions owing to all scattering ways, for the electrons in the lth subband of one valley takes the form

$$\frac{\partial f(\mathbf{p}_l)}{\partial t} = \sum_{\alpha} \sum_{l'} \hbar^{-2} \int d\mathbf{p}'_{l'} f_0(\epsilon_{\parallel,l}) W^0_{\alpha}(i,f) \times [\phi(\mathbf{p}'_{l'}) - \phi(\mathbf{p}_l)][\delta(-\epsilon'_{\parallel,l'} + \epsilon_{\parallel,l} + E_l - E_{l'} + \hbar\omega_{\alpha}) + \delta(-\epsilon'_{\parallel,l'} + \epsilon_{\parallel,l} + E_l - E_{l'} - \hbar\omega_{\alpha}) e^{\hbar\omega_{\alpha}/k_B T} \times \Theta(\epsilon_{\parallel,l} + E_l - \hbar\omega_{\alpha})], \quad (29)$$

where $\Theta(x)$ is the Heaviside step function. The summation over l' in Eq. (29) is performed over all the states in all the subbands, including the lth subband.

The matrix element of the variational method corresponding to the collision term, Eq. (29), is of the form

$$L_l(j,j',\beta,\beta') = \sum_{\alpha} \sum_{l'} L^{\alpha}_{ll'}(j,j',\beta,\beta') \delta_{\beta\beta'}, \quad (30)$$

where

$$L^{\alpha}_{ll'}(j,j',\beta,\beta') = \hbar^{-2} \int d\mathbf{p}_l d\mathbf{p}'_{l'} W^{\alpha}_0(i,f) A^{\alpha}_{ll'}(j,j',\beta,\beta') \times \delta(-\epsilon'_{\parallel,l'} + \epsilon_{\parallel,l} + E_l - E_{l'} + \hbar\omega_{\alpha}), \quad (31)$$

and

$$A^{\alpha}_{ll'}(j,j',\beta,\beta') = [(\epsilon'_{\parallel,l'})^j p'_{l',\beta} - \epsilon^j_{\parallel,l} p_{l,\beta}] \times [(\epsilon'_{\parallel,l'})^{j'} p'_{l',\beta'} - (\epsilon_{\parallel,l})^{j'} p_{l,\beta'}]. \quad (32)$$

All possible transitions of electrons in all the subbands of the valley are described by the matrix element $L(j,j',\beta,\beta') = \Sigma_l L_l(j,j',\beta,\beta')$, that determines the components of the second-rank diagonal tensor of conductivity for the valley, $\sigma_{\beta\beta'} = \Sigma_l (\sigma_{\beta\beta'})_l$, or $\sigma_{\beta} = \Sigma_l (\sigma_{\beta})_l$, according to Eq. (30). Here, $(\sigma_{\beta})_l$ is the specific subband conductivity,

$$(\sigma_{\beta})_l = -\frac{2e^2 [B^{\beta}_{0,l}]^2}{k_B T L_l(0,0,\beta,\beta)} \left\{ L_l(0,0,\beta,\beta) \frac{[L_l(1,1,\beta,\beta) - D^{\beta}_l L_l(1,0,\beta,\beta)] + D^{\beta}_l [L_l(0,0,\beta,\beta) D^{\beta}_l - L_l(1,0,\beta,\beta)]}{L_l(0,0,\beta,\beta) L_l(1,1,\beta,\beta) - [L_l(1,0,\beta,\beta)]^2} \right\}, \quad (33)$$

where $D^{\beta}_l = B^{\beta}_{1,l}/B^{\beta}_{0,l}$, $B^{\beta}_{j,l} = \int d\mathbf{p}_l \epsilon^j_{\parallel,l} v_{\beta} f_{0,l}(\epsilon_{\parallel,l})$, and v_{β} is the β component of the 2D electron velocity. Inelasticity of the scattering is taken into account by the factor in the curly brackets in Eq. (33), while the factor before these brackets determines the conductivity in the relaxation time approximation [note, that one can readily obtain expressions for the relaxation times and conductivities in the relaxation time approximation directly by means of Eq. (19)]. Using Eqs. (30)–(33) it is possible to calculate a conductivity tensor taking into account any different scattering mechanisms as separately as together.

The symmetry consideration dictates that all the equivalent ''oblique'' ellipsoids must share a common value of $\sigma_x^{\langle o \rangle}$ and $\sigma_y^{\langle o \rangle}$, taken for a certain ''oblique'' valley. That is why the conductivity of many-valley system is a scalar which for configurations 1a, 1b, and 2, is given, respectively, by the expressions,

$$\sigma = \sigma_x^{\langle 111 \rangle} = \sigma_y^{\langle 111 \rangle}, \quad (34)$$

$$\sigma = \sigma_y^{\langle 111 \rangle} + \frac{3}{2}(\sigma_x^{\langle o \rangle} + \sigma_y^{\langle o \rangle}), \quad (35)$$

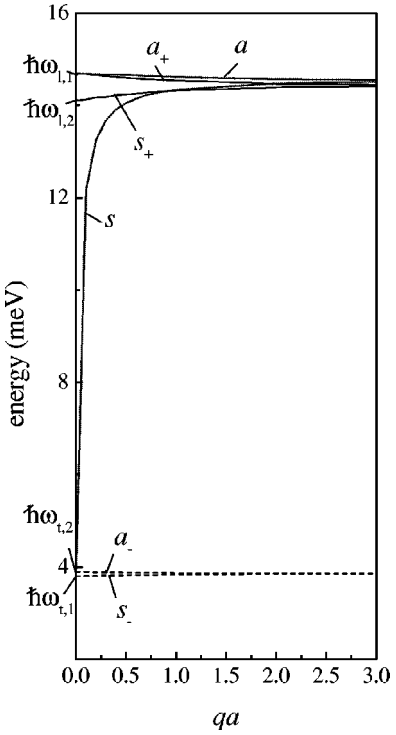

FIG. 2. Spatial dispersion of energy of the IF modes for the PbTe/$Pb_{0.8}Sn_{0.2}$Te/PbTe three-layered structure and of the SO modes for the $Pb_{0.8}Sn_{0.2}$Te FSS. At $q=0$ the energies are equal to the corresponding energies of the usual bulk phonons.

$$\sigma = 2(\sigma_x^{\langle o\rangle} + \sigma_y^{\langle o\rangle}). \tag{36}$$

The in-plane electron mobility is $\mu = \sigma/en$, where n is the total electron density summed over all the valleys.

III. NUMERICAL RESULTS AND DISCUSSION

A. Properties of electron-interface phonon interaction

Through Eq. (13), the value of $(\omega_{l,1}/\omega_\alpha)^{1/2}(\omega_\alpha^2 - \omega_{t,1}^2)/(\omega_{l,1}^2 - \omega_{t,1}^2)$ determines the effectiveness of the electron-IF-phonon interaction. There are two principal regimes of the IF-mode frequencies: (a) $(\omega_{l,1} > \omega_{s+,a+} > \omega_{l,2}) > (\omega_{t,2} > \omega_{s-,a-} > \omega_{t,1})$ is realized in PbTe/Pb_xSn_{1-x}Te and InP/AlSb, or $(\omega_{l,2} > \omega_{s+,a+} > \omega_{l,1}) > (\omega_{t2} > \omega_{s-,a-} > \omega_{t,1})$ is realized in some GaAs/$Al_{0.3}Ga_{0.7}$As (GaAs-type), and (b) $(\omega_{l,2} > \omega_{s+,a+} > \omega_{t,2}) > (\omega_{l,1} > \omega_{s-,a-} > \omega_{t,1})$ is realized in GaAs/AlAs and $Ga_{0.47}In_{0.53}$As/InP (see Fig. 2 here; Fig. 2 in the work by Chen *et al.*;[7] Ref. 6). Thus, an electron in QW interacts much stronger with the s_+, a_+ modes than with the s_-, a_- modes. It is of interest that in case (b) the frequencies of the s_+, a_+ modes are determined by the properties of the barrier layer [as for $Ga_{0.47}In_{0.53}$As/InP QW (Ref. 6)] rather than by the lattice of the QW layer. Contrary to that, in case (a), an electron in the QW interacts only with the modes whose frequencies are close to the frequency of the bulk longitudinal vibrations in the same layer. It is particularly manifested for PbTe/Pb_xSn_{1-x}Te because $\omega_{l,1} \approx \omega_{l,2}$, $\omega_{t,1} \approx \omega_{t2}$ and $\omega_l \gg \omega_t$. To some extent, this is similar to the bulk medium case. However, even if the adjacent lattices have an arbitrary small difference (close values of their ω_l, ω_t, ϵ_∞), the normalization factor for the IF modes

TABLE I. Parameters for $Pb_{1-x}Sn_xTe$ used for the calculations. The values of ϵ_0, ϵ_∞, $\hbar\omega_t$ are chosen to be temperature dependent, satisfying the relations $\epsilon_0/\epsilon_\infty = (\omega_l/\omega_t)^2$ and $\epsilon_0 \propto \alpha(T - T_c)^{-1}$, T_c being a constant. The magnitudes of ϵ_g, $u_\perp$, and $u_\parallel$ are taken from Ref. 40, the others are from Ref. 41. To avoid any uncertainties in the calculations (Ref. 36) the value of ϵ_g is taken for bulk $Pb_{1-x}Sn_xTe$.

	$Pb_{1-x}Sn_xTe$	
Parameter	$x=0$	$x=0.2$
ϵ_0(4.2 K)	1300	6000
ϵ_0(300 K)	430	500
ϵ_∞(4.2 K)	39	53
ϵ_∞(300 K)	33	40
$\hbar\omega_t$(4.2 K), meV	2.4	1.4
$\hbar\omega_t$(300 K), meV	3.9	3.8
$\hbar\omega_l$, meV	14.1	14.7
ϵ_g, meV	$172 - 535x + [12.8^2 + 0.19(k_BT + 20)^2]^{1/2}$	
$u_\perp$, meV	$7320 - 3200\exp(-64[0.35 - x]^2)$	
$u_\parallel$, meV	440	

$$C_{IF} = [3/(\epsilon_{\infty,1}+2)][\epsilon_{\infty,1}(\omega_{l,1}^2 - \omega_\alpha^2) - (\omega_{t,1}^2 - \omega_\alpha^2)]B_\alpha^{-1}\{q/[\sinh(qa)]\}^{1/2}$$

does not vanish. Thus, application of the bulk mode approximation instead of the DCML is valid only for rather big layer thicknesses, when the influence of the surface dipoles at the boundaries on the EPI is negligible.

B. Effect of temperature and QW width on the electron-DCML phonon interaction

We choose a reasonable value of $V_b = 60$ meV because of the uncertainty of the offset value. Our calculations for the $\langle 111\rangle$ valley show that in spite of the small value of V_b, the penetration of the electron wave functions into the barriers is of a few percent for the considered QW widths, which is attributed to a large value of $m_z \approx 0.25m_0$. The in-plane mobility attains rather high values owing to small in-plane effective masses of the electrons in the QW (big value of $u_\perp$, Table I). The electron concentration is required to be smaller than 10^{11} cm^{-2} in order to satisfy the nondegeneration condition for 70 K $< T <$ 300 K.

There is the electrophonon resonance effect (EPR) in two-subband approximation at $a \approx 140$ Å for PbTe/$Pb_{0.8}Sn_{0.2}$Te and at $a \approx 180$ Å for $Pb_{0.8}Sn_{0.2}$Te FSS, which will be analyzed in detail further. Now we deal with the width range with no EPR.

Figures 3 and 4 demonstrate that the intrasubband scattering, rather than the intersubband one, limits the electron mobility. The intrasubband scattering rate is larger than the intersubband one by more than an order of magnitude because of a smaller value of q for the phonons actually interacting with electrons. Note that the magnitudes of q for intervalley transitions are far larger than those for intersubband scattering in one valley.

The interaction with LO modes is a dominant mobility-limiting mechanism in PbTe/$Pb_{0.8}Sn_{0.2}$Te, as well as in the $Pb_{0.8}Sn_{0.2}$Te FSS, when $a > 120$ Å ($a > 230$ Å) at T

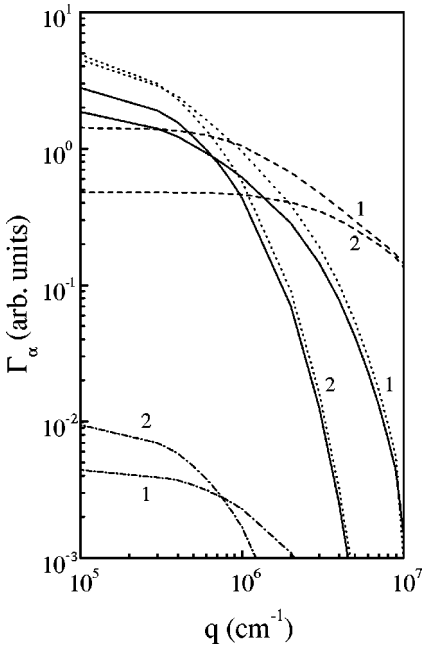

FIG. 3. Dependence of Γ_α upon q for different widths of the $Pb_{0.8}Sn_{0.2}Te$ QW ($1-a=100$ Å, $2-a=300$ Å). Dashes for the LO modes, dots for the s modes, solid lines for the s_+ modes, and dot-dashes for the s_- modes. The factors in Eq. (11) describing the z dependences of Γ_α are assumed to be equal to 1. Only the LO mode with $m=1$ and symmetric interface modes are presented.

$=300$ K(T=77 K), otherwise the interaction with the interface modes becomes the most pronounced (lines 1, 2, and 3 in Figs. 5 and 6).

The polarization field of s mode and its EPI are stronger than those for s_+-mode, Fig. 3, due to different distributions

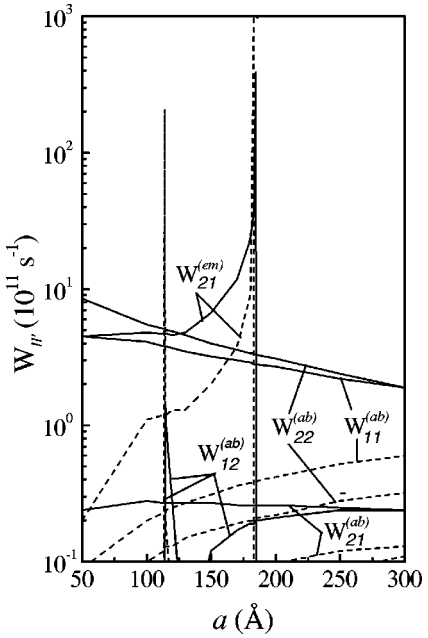

FIG. 4. Scattering rate as a function of the QW width. $\epsilon_{\parallel,1}=\epsilon_{\parallel,2}=5$ meV. Configuration 1a, $\varphi=0$, $T=77$ K. ''em'' and ''ab'' indicate emission and absorption, ''ll''' indicates an electron transition from the lth subband to the l'th one. The meaning of the lines is the same as in Fig. 3. Scattering rates for the other modes are neglected as compared with the presented ones.

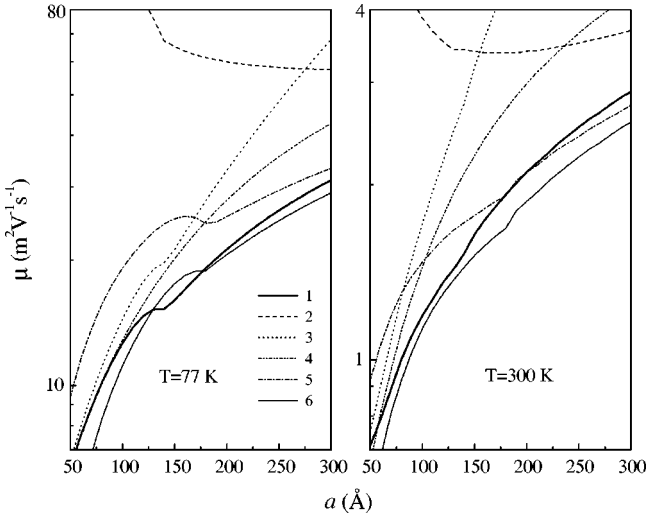

FIG. 5. Mobility as a function of the QW width at $T=77$ K and $T=300$ K. Configuration 1a. Line 1: $PbTe/Pb_{0.8}Sn_{0.2}Te$, $V_b=60$ meV, two-subband system, scattering from the confined LO and IF modes. Line 2: $PbTe/Pb_{0.8}Sn_{0.2}Te$, $V_b=60$ meV, two subbands, LO modes. Line 3: $PbTe/Pb_{0.8}Sn_{0.2}Te$, $V_b=60$ meV, two subbands, IF modes. Line 4: $PbTe/Pb_{0.8}Sn_{0.2}Te$, $V_b=60$ meV, one subband, LO and IF modes. Line 5: $PbTe/Pb_{0.8}Sn_{0.2}Te$, $V_b=\infty$, two subbands, LO and IF modes. Line 6: $Pb_{0.8}Sn_{0.2}Te$ FSS, $V_b=\infty$, two subbands, LO and SO modes.

of the dipoles at the interfaces (see also Ref. 5), in spite of the fact that the frequencies ω_{s+} and ω_s are very close to each other. In order to inspect what is the difference between influence of the s mode and s_+ mode on the mobility, the mobility is calculated in the approximation of infinitely deep QW for both $PbTe/Pb_xSn_{1-x}Te$ and $Pb_{1-x}Sn_xTe$ FSS. Figures 5 and 6 (lines 5 and 6), and Fig. 7 illustrate that this difference is quantitative and essential, particularly for small QW widths.

Although s_- modes (as well as a_- modes) do not contribute to the electron transport (Fig. 6), we will make some

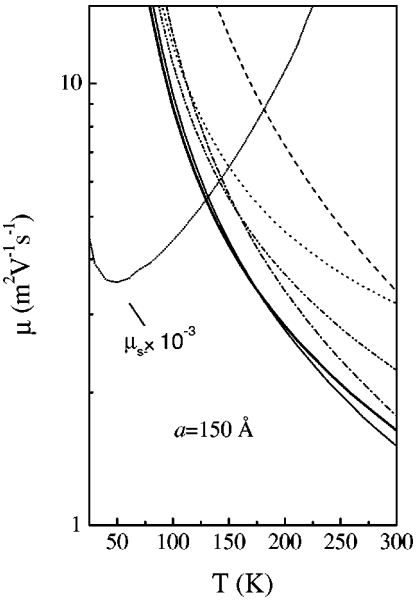

FIG. 6. Temperature dependence of the electron mobilitiy. The meaning of the lines is the same as in Fig. 5.

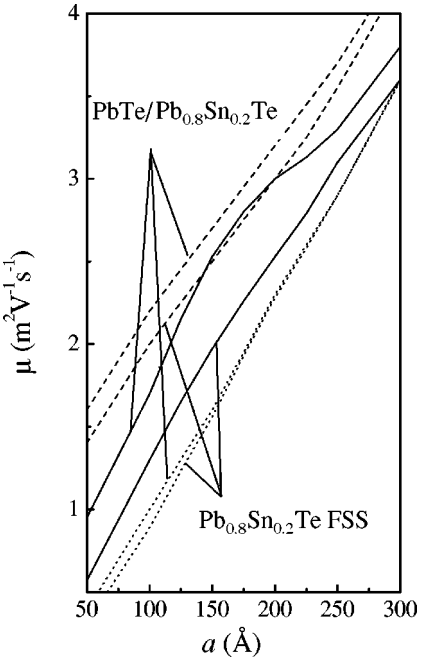

FIG. 7. Electron mobility as a function of the QW width. The electrons occupy the ground subband only. $T=300$ K. Infinitely deep QW approximation. Scattering from the LO and interface modes together. Solid lines for configuration 1a, dots for configuration 1b, dashes for configuration 2.

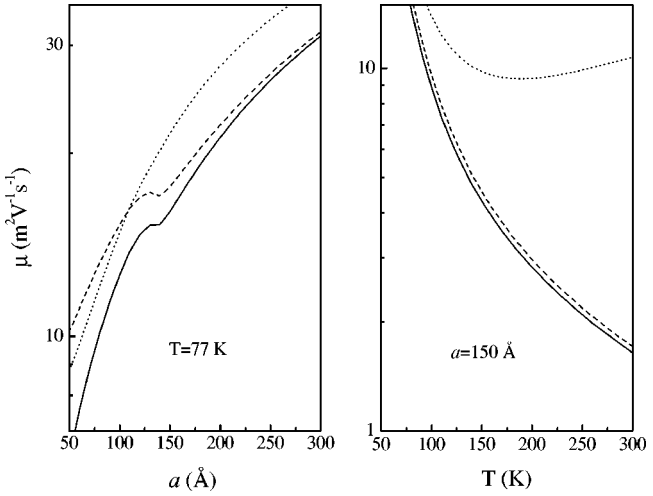

FIG. 8. Illustration of influence of the nonparabolicity on dependence of the mobility vs QW width (at $T=77$ K) and temperature (at $a=150$ Å). Configuration 1a. $PbTe/Pb_{0.8}Sn_{0.2}Te$, $V_b=60$ meV, two-subband system, scattering from the confined LO and IF modes. Solid line for the nonparabolicity approximation (subband nonparabolicity and in-plane effective mass quantization) [by Eqs. (4) and (5)]. Dashes for the subband nonparabolicity approximation [by Eq. (4) with $m^*_{\perp,l}(a)=m^0_\perp$]. Dots for the parabolicity approximation.

comments on an unusual (anomalous) temperature dependence of the calculated mobility limited by the scattering from the s_- mode, μ_{s-}. The reduction of $(\omega_{t,1}-\omega_{t,2})$ with temperature leads to a sharp decrease of $\Gamma_{s-}(T)$, $W_{s-}(T)$, and $\mu_{s-}(T)$. However, we will see that such an anomalous behavior can remain under certain conditions even if all parameters of the materials, including $\omega_{t,1}$ and $\omega_{t,2}$, are independent of temperature. There are always two factors which have growing and opposite influence on motility with increasing temperature: (i) number of phonons, and (ii) number of electrons with higher kinetic energy. Usually the influence of the growing number of phonons is dominant, and the mobility decreases as temperature increases (as for the s_+, a_+, *s*, and *a* modes). Nevertheless, there exists a certain temperature interval where the effect of the growing number of fast electrons becomes predominant that determines an increasing behavior of $\mu_{s-}(T)$ with increasing temperature. It is similar to the Coulomb scattering from the ionized impurity. The only condition for that is that the phonon energy is required to be small enough (less than 10 meV for the considered materials).

C. Effect of nonparabolicity, potential barrier height, electron population of higher subbands, and different configurations of valleys

From Fig. 8 one can conclude that when studying electron transport, the nonparabolicity must be taken into account. Besides, the nonparabolicity in QW systems can be successfully represented as a composition of two contributions: (a) subband nonparabolicity, (b) in-plane mass quantization, whose influences on the mobility can be analyzed separately by Eqs. (4) and (5), respectively. In fact, the subband nonparabolicity represents the nonparabolicity effect on the mobility just for $a>250$ Å, otherwise the in-plane mass quantization effect arises. The influence of the subband nonparabolicity on the mobility becomes noticeable at $T\approx 70$ K and increases with temperature.

Equation (6) directly shows that the velocity effective mass depends upon *a* in infinitely deep QW as well as in QW with finite barriers due to the E_l vs *a* dependence. For comparison see Ref. 6, where different inclination of the $m_{v,1}(\epsilon_{\|,1})$ functions for different QW widths, i.e., the dependence of $m_{v,1}$ upon *a* is explained merely by the different penetration of the electron wave functions into the barriers that have a weaker nonparabolicity than the QW.

Having an effect on the nonparabolicity and overlapping between the electron and phonon wave functions, the magnitude of the potential barrier height, V_b, influences the mobility as a result. Our calculations indicate that a change of nonparabolicity, induced by a change of V_b, affects the mobility much stronger than the induced change of the overlapping. The smaller V_b is, the larger the effective mass becomes owing to the change of the subband nonparabolicity rather than mass quantization. As a result, the mobility decreases weakly when V_b is made smaller, particularly at low temperatures and small *a* (lines 1 and 5 in Figs. 5 and 6). This also gives rise to a far deeper local minimum on the μ vs *a* dependence due to the EPR when $V_b=\infty$ in comparison with that for $V_b=60$ meV. Our calculations for the parabolic case show that μ_{LO} (μ_{IF} and μ_{LO+IF}) increases (decreases) about 2 times when the height changes from $V_b=\infty$ to $V_b=60$ meV.[42]

The interdiffusion of the adjacent layers of $PbTe/Pb_xSn_{1-x}Te$ QW makes the interfaces not perfect, which can cause an asymmetry of QW and violation of the transition rules for the EPI. The calculations show that reasonable asymmetry of QW does not produce a visible change

of the mobility (if the discrepancy between the left and right barrier heights is less than 10%).

Figures 5 and 6 (lines 1 and 4) demonstrate that population of the second subband by electrons induces a mobility decrease in the two-subband system. This means that the mobility of electrons in the second subband is smaller than that in the first one. Effective masses and scattering rates which are larger in the second subband compared to the first one (in the considered intervals of the QW widths and temperatures) are found to be responsible for that. Besides, lines 1 and 4 in Fig. 6 illustrate that the mobility of a many-subband system is essentially affected by the electrons in a higher subband as long as the gap between this subband and the lowest one does not exceed k_BT. The fact that the mobility is actually determined by the intrasubband transitions (beyond the EPR) accounts for this property.

Equations (4), (5), (6), and (9) show that both the subband number and the angle between the QW growth axis and the valley axis affect the effective mass values. In addition, this influence on mobility depends upon the scattering mechanism (here we do not consider the difference between the electron wave functions for the $\langle 111 \rangle$ valley and ''oblique'' valleys). This leads to a difference between electron mobilities in: (i) the $\langle 111 \rangle$ valley and an ''oblique'' one, (ii) a lower subband and a higher one, as shown in Fig. 7. The effect of effective mass quantization gives rise to a considerable reduction of the mobility for configuration 1b compared to that for configuration 1a. The effect of the subband nonparabolicity results in an outstanding increase of the mobility for configuration 2 in comparison with configurations 1b and 1a.

D. Electrophonon resonance effect

Since we consider the two-subband system, the electrophonon resonance effect has to be taken into account. It is predicted by Xu and coworkers[43] that every time as the energy difference between two subbands equals the energy of the LO phonon there is a resonant scattering reducing the mobility, and the conductivity is expected to oscillate as a function of the energy difference. This must affect the dependence of the mobility upon the QW width.

In the two-subband system there exist only two transitions that exhibit a resonance behavior of their scattering rates. (i) Transition with emission from the upper subband to the lower one $(2 \rightarrow 1)$. (ii) Transition with absorption from the lower subband to the upper one $(1 \rightarrow 2)$, with a low kinetic energy of the electrons. The resonance in scattering rate as a function of the QW width (Fig. 4) occurs due to two reasons. The energy conservation law leads to a steplike behavior of QW-width dependence of scattering rates, e.g., $W_{21}^{(\mathrm{em})}(a)$, in the interval $a \geqslant a_0$ (a_0 corresponds to the energy gap $\triangle_{12} = \hbar\omega_\alpha$). On the other hand, it is the dependence of the EPI upon q that reduces $W_{21}^{(\mathrm{em})}(a)$ drastically with decreasing a when $a \leqslant a_0$.

For our two-subband system $\triangle_{12} = \hbar\omega_\alpha$ at $a_0 \approx 140$ Å for PbTe/$Pb_{0.8}Sn_{0.2}$Te and at $a_0 \approx 180$ Å for $Pb_{0.8}Sn_{0.2}$Te FSS with $\alpha = \mathrm{LO}, s_+, a_+, s, a$, Fig. 1.

When a is close to a_0, some of the intersubband transitions become stronger than intrasubband ones, and the scattering $2 \rightarrow 1$ becomes the most effective reason to cause the local minimum appearance on the mobility vs QW-width dependence (Fig. 5). The nonparabolicity makes the local minimum considerably deeper. The EPR is in fact unaffected by temperature.

It is seen from Fig. 5 that the EPR occurs differently for different modes in spite of their close frequencies. Two main distinctions exist: (a) between the EPR for the confined LO and the interface (IF and SO) modes; (b) between the EPR for s_+, a_+ modes and s, a modes. The first distinction is caused by the stronger QW-width dependence of the EPI for the interface modes as compared with that for the LO modes; the EPR for the interface modes is smoothed. The second distinction is given rise to the stronger polarization field of the SO modes compared to the IF modes.

It is interesting to compare the depth of the resonances on the dependencies μ vs a presented here with the results of Xu *et al.*[43] where the phonons are considered as usual bulk LO modes. In Ref. 43 the conductivity changes are about 30% at the EPR, while in our case such changes do not exceed 15% for the scattering from the LO, IF, and SO modes separately as well as from the LO and interface modes together. The scattering from the confined LO modes for $V_b = \infty$ produces the mobility change of about 30%.

Finally, we make some remarks concerning the oscillation of $\mu(a)$ predicted in Ref. 43. Generally, $\mu_\alpha(a)$ might be expected to have such an oscillation, i.e., to have a number of local minima when energy gap between some pair of the subbands equals to $\hbar\omega_\alpha$. This leads to a series of $a_{0,i}$. However, there are two reasons hindering the oscillation. Firstly, for a being far enough from $a_{0\,i}$, the intrasubband scattering is the controlling factor. Secondly, the most pronounced EPR is caused by transitions between the lowest subband and the second one, while the upper subbands do not participate actively in the transport because of a much smaller density of the electrons in them. Nevertheless, there could be another possibility for the oscillation for a QW with a number of phonon modes with rather distant frequencies. Such resonances in the transitions $2 \rightarrow 1$ could be expected to be rather deep.

The EPR could be observed in the mobility dependence upon the external pressure applied to QW since the pressure affects the gap between the subbands.

IV. CONCLUSIONS

The most important results obtained in this paper can be summarized as follows.

(1) The electrons in the QW layer of PbTe/Pb_xSn_{1-x}Te/PbTe interact virtually only with the phonon modes with frequencies close to that of bulk longitudinal vibrations of the same layer.

(2) The dominant mobility-limiting mechanism is the scattering from the confined LO modes if the QW width exceeds 120 Å (230 Å) at 300 K (77 K), otherwise the IF modes dominate. The phonon engineering is not applicable.

(3) It is shown that the nonparabolicity of the electron energy dispersion law in a QW can be effectively reduced to the two separate effects: (a) the subband nonparabolicity, (b) the in-plane effective mass quantization.

(4) The energy dispersion law of the low-subband elec-

trons in $Pb_xSn_{1-x}Te$ QW is essentially nonparabolic. Influence of the nonparabolicity on the mobility is actually represented by the subband nonparabolicity alone if the QW width exceeds 250 Å, otherwise the in-plane mass quantization effect arises.

(5) The increase of barrier height causes the mobility growing due to mainly weakening subband nonparabolicity.

(6) The mobility of many-subband system is limited mostly by the intrasubband scattering (beyond the EPR). The mobility of the electrons in a higher subband is smaller than that in the first one because of a larger effective mass and bigger scattering rates in a higher subband. Electrons in a higher subband essentially affect the mobility if the gap between their subband and the ground one does not exceed k_BT.

(7) A considerable difference between the mobilities for QW structures with different growth axes is caused by different effects of the subband nonparabolicity and the in-plane mass quantization in them.

(8) The electrophonon resonance effect is determined mainly by the transitions of electron from the second subband to the first one accompanied by phonon emission. The subband nonparabolicity makes the resonance sharper. There is a local minimum on the QW-width dependence of the mobility due to the EPR. This minimum occurs at the width near 140 Å for $PbTe/Pb_xSn_{1-x}Te$ and 180 Å for $Pb_{0.8}Sn_{0.2}Te$ FSS, with the $\langle 111 \rangle$ growth axis.

ACKNOWLEDGMENTS

The author would like to thank V. A. Shenderovskij, F. F. Sizov, and M. Załużny for stimulating discussions, and S. Odoulov and V. Pergamenshchik for their critical reading of the paper.

*Electronic address: bondaren@iop.kiev.ua

[1] I. Dharssi and P. N. Butcher, J. Phys.: Condens. Matter **2**, 119 (1990).
[2] I. Dharssi, P. N. Butcher, and G. Warren, Superlattices Microstruct. **9**, 335 (1991).
[3] R. P. Joshi, J. Appl. Phys. **71**, 3827 (1992).
[4] N. Mori and T. Ando, Phys. Rev. B **40**, 6175 (1989).
[5] K. W. Kim, M. A. Stroscio, A. Bhatt, R. Mickevicius, and V. V. Mitin, J. Appl. Phys. **70**, 319 (1991).
[6] S. Mukhopadhyay and B. R. Nag, Phys. Rev. B **48**, 17 960 (1993).
[7] R. Chen, D. Lin, and T. F. George, Phys. Rev. B **41**, 1435 (1990); X. Liang and X. Wang, *ibid.* **43**, 5155 (1991); Refs. 3 and 4.
[8] G. Fishman, Phys. Rev. B **36**, 7448 (1987).
[9] X. T. Zhu, H. Goronkin, G. N. Maracas, R. Droopad, and M. A. Stroscio, Appl. Phys. Lett. **60**, 2141 (1992).
[10] H. Rucker, E. Molinary, and P. Lugli, Phys. Rev. B **44**, 3463 (1991); **45**, 6747 (1992).
[11] G. Weber, A. M. de Paula, and J. F. Ryan, Semicond. Sci. Technol. **6**, 397 (1991).
[12] C. Guillemot and F. Clerot, Phys. Rev. B **44**, 6249 (1991).
[13] H. Leon and F. Comas, Phys. Status Solidi B **160**, 105 (1990).
[14] H. Leon, F. Leon, and F. Comas, Phys. Status Solidi B **170**, 449 (1992).
[15] M. A. Stroscio, J. Appl. Phys. **80**, 6864 (1996).
[16] J. Pożela, V. Juciene, N. Namajùntas, and K. Pożela, in *Proceedings of the 23rd International Conference on the Physics of Semiconductors*, edited by M. Scheffier and R. Zimmermann (World Scientific, Singapore, 1996), p. 2391.
[17] J. Wang, J. P. Leburton, and J. Pożela, J. Appl. Phys. **81**, 3468 (1997).
[18] J. Pożela, V. Juciene, and K. Pożela, Semicond. Sci. Technol. **10**, 1595 (1995); Lith. Phys. J. **36**, 149 (1996).
[19] G. Bastard, *Wave Mechanics Applied to Semiconductor Heterostructures* (Les Editions de Physique, Les Ulis, 1988).
[20] M. de Dios Leyva and J. Lòpez-Gondar, Phys. Status Solidi B **138**, 253 (1986).
[21] G. Paasch, P. H. Nguyen, and G. Gobsch, Phys. Status Solidi B **162**, 155 (1990).
[22] B. R. Nag, Appl. Phys. Lett. **59**, 1620 (1991).
[23] V. K. Dugaev and P. P. Petrov, Phys. Status Solidi B **184**, 347 (1994).
[24] A. M. Alcalde and G. Weber, Solid State Commun. **96**, 763 (1995).
[25] D. F. Nelson, R. C. Miller, and D. A. Kleinman, Phys. Rev. B **35**, 7770 (1987).
[26] B. R. Nag and S. Mukhopadhyay, Phys. Status Solidi B **175**, 103 (1993).
[27] U. Ekenberg, Phys. Rev. B **36**, 6152 (1987).
[28] C. Wetzel, R. Winkler, D. Drechsler, B. K. Meyer, U. Rosler, J. Scriba, J. P. Kotthaus, V. Harle, and F. Scholz, Phys. Rev. B **53**, 1038 (1996).
[29] W. Okulski and M. Załużny, Thin Solid Films **204**, 239 (1991).
[30] V. V. Bondarenko, V. A. Shenderovskij, and V. V. Teterkin, Ukr. Phys. J. **36**, 314 (1991).
[31] F. F. Sizov and A. Rogalski, Prog. Quantum Electron. **QE-17**, 3 (1993).
[32] A. Ishida, S. Matsuura, H. Fujiyasu, H. Ebe, and K. Shinohara, Superlattices Microstruct. **2**, 575 (1986).
[33] G. Bauer, Surf. Sci. **168**, 462 (1986).
[34] S. V. Plyatsko, Yu. S. Gromovoj, G. E. Kostyunin, and V. P. Kladko, Thin Solid Films **221**, 127 (1992).
[35] V. V. Bondarenko and F. F. Sizov, Phys. Low-Dimens. Semicond. Struct. **8/9**, 123 (1995); Inorg. Mater. **33**, 178 (1997).
[36] M. V. Valeiko, I. I. Zasavitskij, A. V. Matveenko, B. N. Matsonashvili, and Z. A. Rukhadze, Superlattices Microstruct. **9**, 195 (1991).
[37] M. Kriechbaum, K. E. Ambrosch, E. J. Fantner, H. Clemens, and G. Bauer, Phys. Rev. B **30**, 3394 (1984).
[38] In the case of an arbitrary ''oblique'' valley, the relation for $\Psi_l(\mathbf{k}_l, z)$ should include a specific prefactor which is neglected in our approach, see M. Załużny, Phys. Rev. B **39**, 12 948 (1989), Ref. 21.
[39] On apllicability of the variational method to description of the optical phonon scattering with its step-like dependence on the transfered energy, see, e.g.: M. N. Griror'ev, I. M. Dykman, and P. M. Tomchuk, Fiz. Tverdogo Tela **7**, 3378 (1965) [Sov. Phys. Solid State **7**, 2719 (1966)]; P. M. Tomchuk, Ukr. Phys. J. **13**, 1369 (1968) (in Russian); P. N. Gavaleshko, P. N. Gorley, V. A. Shenderovskij, L. S. Solonchuk, and P. M. Tomchuk, Phys. Status Solidi B **71**, 41 (1975); P. N. Gorley and V. A. Shenderovskij, *Variational Method in Kinetic Theory* (Naukova Dumka, Kiev, 1992) (in Russian).

[40] A. Rogalski and K. Jożwikowski, Phys. Status Solidi A **111**, 559 (1989).

[41] A. V. Lubchenko, E. A. Salkov, and F. F. Sizov, *Physical Basis of Semiconductor Infrared Photoelectronics* (Naukova Dumka, Kiev, 1984) (in Russian).

[42] The materials with much higher barrier heights than that in $PbTe/Pb_xSn_{1-x}Te$ are $PbTe/Pb_{1-x}Eu_xTe_{1-y}Se_y$, $PbTe/Pb_{1-x}Eu_xTe$.

[43] W. Xu, F. M. Peeters, and J. T. Devreese, Phys. Rev. B **48**, 1562 (1993).